Biointerphases

RESEARCH ARTICLE | JULY 11 2025

Enhanced collagenogenesis on three-dimensionally printed titanium surfaces by human gingival fibroblasts: An *in vitro* study

Vitor de Toledo Stuani ; Isabela Sanches Pompeo da Silva ; Gustavo Gonçalves do Prado Manfredi ; Fernanda Balestrero Cassiano ; Larissa Alamo ; Ligia Espoliar Corrêa ; Jamil Awad Shibli ; Carlos Alberto de Souza Costa ; Diana Gabriela Soares

Biointerphases 20, 041002 (2025)
https://doi.org/10.1116/6.0004500

Biointerphases
A Journal of Biomaterials and Biological Interfaces

ARTICLE

pubs.aip.org/avs/bip

Enhanced collagenogenesis on three-dimensionally printed titanium surfaces by human gingival fibroblasts: An *in vitro* study

Cite as: Biointerphases 20, 041002 (2025); doi: 10.1116/6.0004500
Submitted: 17 February 2025 · Accepted: 11 June 2025 ·
Published Online: 11 July 2025

Vitor de Toledo Stuani,[1] Isabela Sanches Pompeo da Silva,[1] Gustavo Gonçalves do Prado Manfredi,[1] Fernanda Balestrero Cassiano,[1] Larissa Alamo,[1] Ligia Espoliar Corrêa,[1] Jamil Awad Shibli,[2,3] Carlos Alberto de Souza Costa,[4] and Diana Gabriela Soares[1,a)]

AFFILIATIONS

[1]Department of Operative Dentistry, Endodontics and Dental Materials, Bauru School of Dentistry, University of Sao Paulo (USP), Sao Paulo 17012-901, Brazil
[2]M3 Health Indústria e Comércio de Produtos Médicos, Odontológicos e Correlatos S.A., Jundiaí 13212-213, Brazil
[3]Department of Periodontology, Dental Research Division, Guarulhos University, Guarulhos 07023-070, Brazil
[4]Department of Physiology, School of Dentistry, University of São Paulo State, UNESP, Araraquara 14801-385, Brazil

[a)]**Author to whom correspondence should be addressed:** soares.dg@usp.br

ABSTRACT

The lack of cementum in peri-implant tissues leads to a deficiency in anchorage points for gingival collagen fibers. This arrangement is linked to reduced protective capabilities compared to teeth. Therefore, there is a pressing need to develop surfaces that optimize the interaction between soft tissue and implants. 3D-printed titanium disks (Ti3DP), machined disks (TiMC), and glass coverslips (GS) were seeded with human gingival fibroblasts. These specimens underwent mechanical characterization via roughness and wettability assays. Biological characterization included assessments of cellular viability (live/dead), adhesion and spreading (F-actin), cell count (DAPI), cellular metabolism (Alamar blue), adhesive strength, and soluble collagen and total protein quantification up to 14 days. Data analysis employed Student's t-test and ANOVA post-hoc Tukey test ($\alpha = 0.05$). The group TiMC exhibited higher hydrophilicity and lower roughness compared to Ti3DP. All groups demonstrated cellular viability throughout the study period. Adhesive strength did not significantly differ among groups; however, cell count was higher in TiMC and GS after one day of cell seeding in comparison to Ti3DP. Morphologically, GS and TiMC displayed more fusiform cells with a uniform distribution, while Ti3DP showed smaller, irregular cells with multiple lamellipodia and filopodia. Additionally, statistically superior collagen and total protein deposition was observed in Ti3DP ($p < 0.01$). The 3D-printed titanium surface allowed human gingival fibroblasts to adhere to it, leading to a 3D cytoskeleton morphology that culminated in increased collagen expression. Therefore, these 3D-printed devices present a promising avenue for producing transmucosal components due to their increase in collagen production.

I. INTRODUCTION

Currently, dental implants have solidified their position as a reliable therapeutic approach for oral rehabilitation.[1] This advancement is largely attributed to the refined comprehension of alveolar remodeling processes and the phenomenon of osseointegration.[1] As a result, over the past decades, both academia and industry have fervently pursued the optimization of implant surfaces to accelerate and improve osseointegration.[2–5] However, equal attention has not been devoted to investigating the establishment of the soft tissue-implant interface.[6] Thus, while technological progress has enabled the development of highly favorable surfaces for osseointegration, one of the main challenges confronting the forthcoming generation of implants lies in enhancing the integration of supracrestal tissues within the implant system.[7]

The interaction between implants and connective tissue during the formation of supracrestal insertion begins at the moment the transmucosal component is installed. This process is guided by both the substrate surface properties and the coordinated activity

of fibroblasts, extracellular matrix, inflammatory cells, and cytokines.[1–3] This integration is a functional and biological parameter essential for providing a protective zone that prevents apical epithelial growth, providing support to peri-implant tissues, enhancing aesthetics, ensuring sealing against microorganisms, and preserving the crestal bone level.[8] Thus, adequate soft tissue sealing can act as a clinical strategy to ensure greater treatment stability while reducing the likelihood of aesthetic-functional issues, such as peri-implantitis and recessions.[8]

Several findings suggest that the topography of the transmucosal component may influence the configuration and composition of the supracrestal soft tissue around implants.[7,9–12] The use of rough or microgrooved surfaces can modify the pattern of insertion of gingival fibers into the transmucosal component and even the proportion of collagen in the connective tissue.[3,13] While the connective tissue surrounding teeth is composed of 60% collagen fibers and approximately 15% fibroblasts, around implants, it is composed of 85% collagen fibers and only up to 3% fibroblasts. For this reason, collagen deposition in the transmucosal sites assumes significant importance since it is a key factor for extracellular matrix synthesis and effective connective tissue formation.[7] Therefore, surfaces capable of stimulating enhanced extracellular matrix deposition in peri-implant areas may contribute to the initial soft tissue adherence to implant surfaces, preventing epithelial apical migration and peri-implantitis.[14]

Additive manufacturing techniques, such as 3D-printing, are gaining traction within the biomedical field. Although still in its early stages, this technology is already being applied in various medical and dental scenarios, particularly for producing implants with complex shapes and controlled roughness and porosity.[5,12] Among these techniques, laser metal fusion (LMF) stands out for its ability to directly manufacture parts from three-dimensional model data by fusing metal powder particles layer by layer.[5,12] The use of 3D-printed titanium surfaces have proven to be competent in the osseointegration process, yet few studies have explored their interaction with soft tissues.[12,15]

Considering these arguments, this study conducted an *in vitro* biological characterization of titanium samples produced via 3D-printing (LMF). The hypothesis proposed is that surface alterations resulting from the manufacturing and post-treatment processes enhance fibroblast activity compared to machined surfaces.

II. MATERIALS AND METHODS

A. Experimental groups

In this study, 3D-printed titanium disks (Ti6Al4V) and machined disks (Ti3DP and TiMC, respectively; Plenum Bioengineering, Brazil) with 12 mm diameter and 2 mm height were compared. TiMC disks were produced via subtractive manufacturing, whereas Ti3DP disks were fabricated using LMF technique (Fig. 1). Postprinting, Ti3DP disks underwent proprietary surface treatment involving blasting and acid etching. Glass coverslips (GS) served as negative controls. Before biological characterization, titanium disks were sterilized with gamma radiation, and glass coverslips were decontaminated using 70% alcohol.

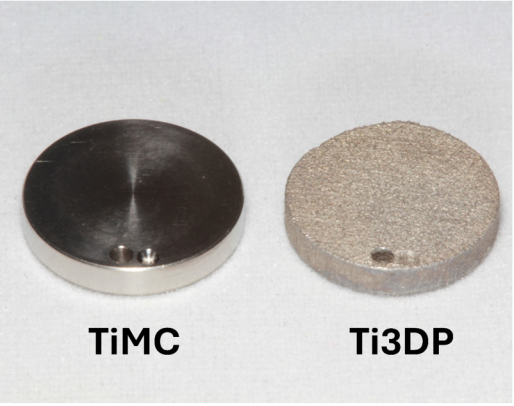

FIG. 1. Representative images of the machined (TiMC) and 3D-printed (Ti3DP) surfaces.

B. Titanium disks' surface characterization

1. Topography

The samples were mounted on aluminum stubs and sputter-coated with gold-palladium (Detron Vacuum—Desk IV, Moorestown, USA). Representative images of each specimen were obtained from the center of each sample using a scanning electron microscope (JSM-T220 A, JEOL Inc., Japan) at magnifications of 50×, 100×, and 1000×.

2. Wettability

Wettability was assessed using sessile drop technique. A 10 μl ultrapure water drop was placed on each sample (n = 6) at 24 °C. After 60 s, a photo was taken to measure the contact angles using ImageJ software (NIH, USA) with the contact angle plug-in [Fig. 1(b)]. Each sample was tested three times for consistency. The analysis was conducted by a single operator, with calibration on 20% of the samples and a 1-month interval between measurements, yielding an intraclass correlation coefficient of 0.91.

3. Surface roughness

Surface roughness (n = 6) was evaluated using a portable roughness tester (Hommel Tester T1000; Jenoptik AG, Jena, Germany). Six readings were taken per sample, spaced at 60° intervals from the center outward. Roughness values were measured as the arithmetic mean (Ra) and the total profile maximum height (Rmax).

C. Biological characterization

1. Experimental design

The experimental model used primary human gingival fibroblasts (HGFs) cultured from gingival tissue around sound third molars from a single donor (18 years), following ethics approval (CAAE protocol #53489421.9.0000.5417). The patient signed informed consent. The tissue was aseptically collected and incubated in 3 mg/ml collagenase type 1 (Sigma-Aldrich, USA) for 4 h at 37 °C and 5% CO_2.

Postdigestion, cells were incubated in six-compartment plates with Dulbecco's Modified Eagle Medium (DMEM) (Gibco, USA) supplemented with 10% fetal bovine serum (FBS) and 1% antibiotic-antimycotic (Sigma, USA) until 80% confluence was reached. The cells from passages 2–6 were used. Disks were placed in 24-well plates, sealed with a silicone ring, to prevent cell displacement. Fibroblasts were seeded at 5×10^4 cells/well in 100 μl of the medium and incubated for 30 min at 37 °C and 5% CO_2 for initial adhesion. An additional 700 μl of the medium was then added, and cultures were maintained for up to 14 days.

2. Cellular viability (live/dead)

At 1, 3, 7, and 14 days (n = 2), the samples were washed with phosphate-buffered saline (PBS) and incubated for 10 min in DMEM containing 4 mM calcein AM and 2 mM ethyl homodimer-1 (Live/Dead cell viability/cytotoxicity kit; Invitrogen). Fluorescence microscopy (FLoid Cell Imaging Station, Applied Biosystems, USA) was used to capture three images per sample (n = 2).

3. Cellular metabolism (Alamar blue)

Samples (n = 6) were incubated at 37 °C and 5% CO_2 for 3 h in DMEM without FBS containing 10% Alamar Blue reagent (Life Technologies, USA) at a 10:1 ratio. After incubation, the supernatant was transferred to a 96-well plate (Corning®, USA), and fluorescence was measured at 540 nm excitation and 590 nm emission (Synergy H1, Biotek, USA). The GS group (glass coverslips) served as a reference for 100% cell proliferation, and results were normalized to the cell count.

4. Cell count

The disks (n = 6) were transferred to a 48-well plate after 1, 3, 7, and 14 days of cell culture, washed with PBS, and fixed in 4% paraformaldehyde (Sigma-Aldrich) for 15 min. Subsequently, the disks were washed in PBS, incubated for 5 min with DAPI mounting medium (Life Technologies, USA) to stain the cell nuclei, and assessed using a fluorescence microscope (FLoid Cell Imaging Station, Applied Biosystems, USA). Three images of each sample were captured at 20× magnification in the central region of the samples. The images were imported into ImageJ software (NIH, USA), and the cell count was determined using the particle counting plug-in.

5. Adhesive fraction

After 1 and 14 days of incubation at 37 °C and 5% CO_2, cellular metabolism of the samples (n = 6) was assessed using the Alamar Blue assay. The samples were then washed twice with PBS, stabilized on an orbital shaker at 200 rpm for 5 min, and washed three more times with PBS to remove detached cells. They were reincubated in Alamar Blue solution. The adhesion fraction was calculated using the formula:[16] *Adhesion fraction = Fluorescence after shaking ÷ Fluorescence before shaking.*

6. Cell adhesion and spreading (F-actin)

The samples were washed with PBS, fixed in 4% paraformaldehyde (Sigma-Aldrich) for 15 min, and then washed twice in PBS. They were incubated for 5 min in 0.1% Triton X-100 (Thermo Fisher Scientific, USA), washed twice again, and incubated with Alexa Fluor Phalloidin 488 in PBS (1:1000; Life Technologies, USA) for 20 min. After another PBS wash, these samples were transferred to a glass slide, treated with DAPI mounting medium (Life Technologies) for 5 min, and evaluated using a confocal microscope (Leica TCS SPE; Leica Microsystems, Germany). Three images per sample (n = 2) were captured.

7. Soluble collagen and total protein quantification

Soluble collagen quantification was performed using the Soluble Collagen Quantification Assay Kit (CS0006, Sigma-Aldrich, USA) (n = 6). The samples, collected from a 48-well plate at 4 and 7 days of cell culture, were stored at −20 °C. After thawing, the medium was centrifuged at 10 000 g for 15 min at 4 °C to remove cells and debris. Half of the supernatant was used for soluble collagen quantification and half for total protein quantification.

For collagen quantification, the supernatant was mixed with Digest Enzyme and Assay Buffer and incubated for 1 h at 37 °C. Collagen peptides were labeled with a fluorescent probe incubated for 5 min at 37 °C, and then Development Solution was added and incubated for 15 min. Fluorescence was measured at 375 nm excitation and 465 nm emission (Synergy H1, Biotek, USA), and the results were normalized to the cell count.

For total protein quantification, supernatants were mixed with 0.1% sodium dodecyl sulfate (Sigma-Aldrich, USA) and incubated for 40 min at room temperature. Lowry solution was added and incubated for 20 min in the dark, followed by Folin reagent and an additional 30 min incubation. Absorbance was measured at 655 nm (Synergy H1, Biotek, USA), and the results were normalized to the cell count using a standard curve with Protein Standard (P5619-1VL; Sigma-Aldrich, USA).

D. Statistical analysis

Statistical analyses were conducted using Jamovi software (Jamovi, Sydney, Australia) with $\alpha = 0.05$ and $\beta = 0.95$. Data from three independent experiments were analyzed using Levene's test and Shapiro–Wilk test (both $\alpha = 0.05$). Two-way ANOVA with post-hoc Tukey test was used to compare group differences and time points, while the ANOVA with post-hoc Tukey test was employed for comparisons only between groups ($\alpha = 0.05$).

III. RESULTS

A. Surface characterizations

Representative SEM micrographs of the analyzed surfaces are shown in Fig. 2. The GS demonstrated a smooth and homogeneous surface with minimal detectable topographical variations. In contrast, the TiMC exhibited well-defined concentric lines attributed to the machining process, indicating a relatively uniform and regular surface pattern. The Ti3DP displayed a markedly rough and irregular morphology, with numerous pores and surface discontinuities consistent with the characteristics of additive manufacturing techniques.

The GS group presented the lowest contact angle (36.86° ± 0.94°), followed by TiMC (65.49° ± 4.02°) and Ti3DP (87.8° ± 7.07°), with

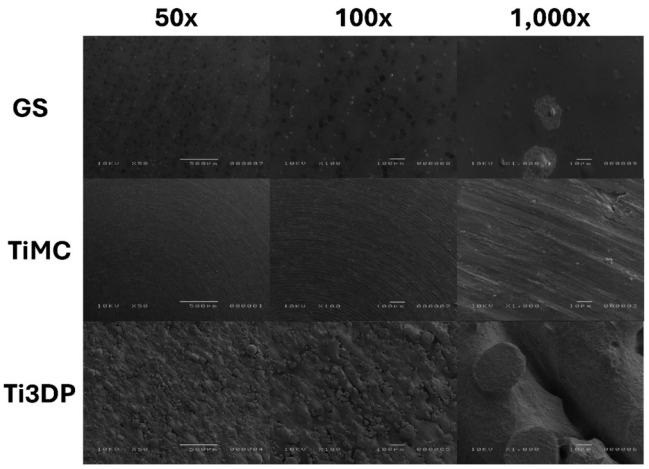

FIG. 2. Representative scanning electron microscopy (SEM) images of the tested surfaces: Glass slide (GS), machined titanium disk (TiMC), and 3D-printed titanium disk (Ti3DP). Images were acquired at magnifications of 50×, 100×, and 1000×.

statistically significant differences observed among all groups ($p < 0.01$) (Fig. 3). These results indicate that GS exhibited the highest surface hydrophilicity, while Ti3DP was the least hydrophilic. Although Ti3DP displayed a higher contact angle, all surfaces maintained values within the hydrophilic range. The Ra parameter was nearly 40 times higher for 3TiDP than TiMC ($7.76 \pm 0.89\,\mu$m versus $0.197 \pm 0.06\,\mu$m, respectively; $p < 0.001$), indicating that the 3D-printing process and the postprinting surface treatment resulted in a significantly rougher surface [Fig. 4(a)]. Similarly, the Rmax parameter was markedly higher in 3TiDP compared to TiMC (47.9 ± 4.27 vs $2.2 \pm 1.38\,\mu$m, respectively; $p < 0.001$) [Fig. 4(b)]. The GS group exhibited the lowest roughness values, with Ra of $0.105 \pm 0.117\,\mu$m and Rmax of $0.0912 \pm 0.0162\,\mu$m. No statistically significant differences were observed between GS and TiMC for either Ra or Rmax, highlighting the smoother surface characteristics of these two groups compared to 3TiDP.

B. Cellular viability, cell metabolism, cell count, and adhesive fraction

In all experimental groups, cells exhibited sustained viability and proliferation over time [Fig. 5(a)]. This observation suggests that the 3D-printing technique did not compromise the biocompatibility. However, a lower cell density was noted in Ti3DP compared to GS and TiMC. Furthermore, noticeable disparities in cell morphology and distribution were evident among the groups. While GS and TiMC displayed similar characteristics with elongated and parallel cells, Ti3DP exhibited a more irregular pattern and a less organized cell distribution. Concerning cell metabolism, no significant differences were observed between TiMC and Ti3DP at any of the assessed time points ($p > 0.05$) [Fig. 5(b)]. Additionally, only in the 1-day analysis was cellular metabolism in TiMC and Ti3DP higher than in GS ($p < 0.05$), possibly due to an initial stress of fibroblasts in contact with titanium. Regarding cell count, across all groups, a similar pattern of cell proliferation was observed, characterized by an initial increase in cell numbers up to day 7, followed by a subsequent reduction on day 14 [Fig. 5(c)]. Notably, a significant difference was observed only on the first day between GS and TiMC ($p < 0.05$), with no discernible difference between TiMC and Ti3DP ($p > 0.05$). However, at subsequent time points, Ti3DP consistently exhibited a significantly lower number of cells compared to GS and TiMC ($p < 0.05$) [Fig. 5(d)]. Regarding adhesive fraction, no difference was observed between Ti3DP, TiMC, and GS at 1 (0.69 ± 0.24, 0.70 ± 0.25, and 0.62 ± 0.10, respectively) and 14 days (0.83 ± 0.11, 0.78 ± 0.16, and 0.66 ± 0.09, respectively) [$p > 0.05$, Fig. 5(e)].

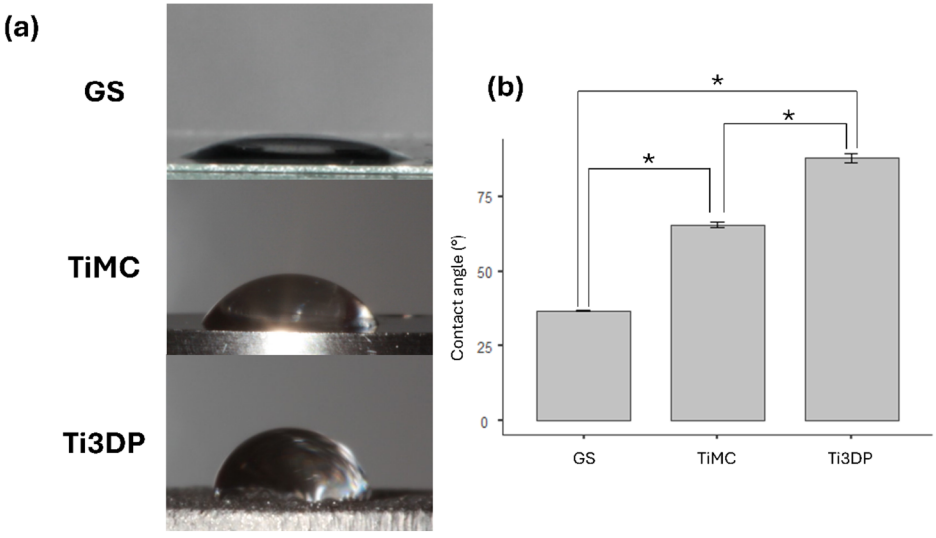

FIG. 3. Wettability assay using the sessile drop technique. (a) In the TiMC group, a more spread-out droplet with a smaller contact angle is observed, indicating higher hydrophilicity. Meanwhile, in the Ti3DP group, the droplet exhibits a contact angle closer to 90°, indicating lower hydrophilicity. On the GS surface, the water droplet appears widely spread with a flattened profile, indicating high surface wettability. (b) All surfaces exhibited hydrophilic behavior; however, TiMC showed significantly lower contact angles compared to Ti3DP, while GS displayed the lowest values among all groups (ANOVA post-hoc Tukey's test, *$p < 0.01$; $n = 6$).

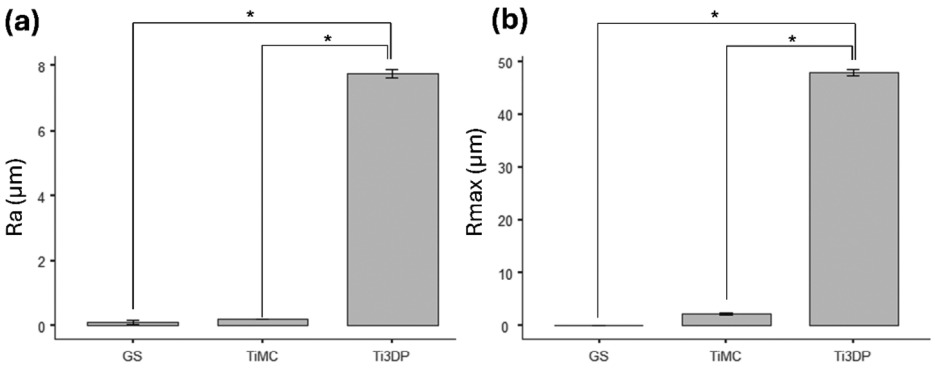

FIG. 4. Roughness assessment. (a) Ra = arithmetic mean of the absolute distances of the roughness profile. (b) Rmax = difference between the highest peak and the deepest valley. (ANOVA post-hoc Tukey's test, *p < 0.001; n = 6).

C. Cell adhesion and spreading

Cell distribution and morphology differed between the groups [Figs. 6(a)–6(d)]. The cytoskeleton architecture in TiMC is characterized by an organized distribution, with elongated and parallel cells following the grooves of the machined disk surface. Additionally, a higher cell density is noted, leading to cell overlap at later analysis times (7 and 14 days). Contrastingly, in Ti3DP, titanium granules stained by the probe can be observed, alongside irregularly shaped fibroblasts intertwining between these spaces. Furthermore, a notable three-dimensionality in cell spreading is observed, with cells arranged at varying vertical levels along the surface, effectively filling the crests and valleys of the samples.

D. Soluble collagen and total protein quantification

Ti3DP exhibited a higher soluble collagen quantification compared to TiMC and GS, with no difference between them ($10.00 \times 10^{-4} \pm 0.82 \times 10^{-4}$, $5.48 \times 10^{-4} \pm 0.90 \times 10^{-4}$, and $5.63 \times 10^{-4} \pm 0.87 \times 10^{-4}$ μg/ml, respectively; Fig. 7(a)). Similarly, the total protein concentration showed the same distribution pattern [0.12 ± 0.08, 0.03 ± 0.01, and 0.03 ± 0.004 μg/ml, respectively; Fig. 7(b)].

IV. DISCUSSION

Dental implant systems intimately interact with three distinct tissues: The epithelium, connective tissue, and bone. The absence of adhesion between the connective tissue and the transmucosal component stands as a significant factor in implant failure.[17] This aspect gains particular importance when considering the relatively fragile nature of the peri-implant complex compared to the periodontium.[18] Some studies propose that homogeneous roughness can facilitate the formation of a peri-implant barrier.[19] 3D-printing has arrived as an alternative for promoting interesting controlled microtextured surfaces, with interesting found being achieved on osteoblasts phenotype modulation, and improved osseointegration.[20–25] Currently, titanium alloys remain the primary focus of investigation for 3D-printed dental implant production, especially Ti6Al4V.[26,27] Several groups have demonstrated the feasibility of producing implants using additive manufacturing techniques, even achieving success and survival rates comparable to those obtained with conventional processes.[10,23,28,29] Furthermore, metal 3D-printing has also been explored in the production of transmucosal components with controlled roughness to enhance the cellular environment of peri-implant soft tissue.[10,15] Therefore, in the present investigation, the effect of 3D-printed Ti6Al4 V alloy processed by selective laser sintering was tested as a bioactive surface to modulate collagen expression by gingival fibroblasts.

According to the SEM images, 3D-printed samples featured a surface topography composed by microgrooves and cavities (Fig. 2). As highlighted by several authors,[27,28] products obtained through 3D-printing technology exhibit certain surface discontinuities that spontaneously generate a microgroove pattern. This characteristic configuration arises from two phenomena. First, the gradual material deposition along the Z axis (vertical) during the printing process results in the presence of distinct layers as the printing step progresses vertically according to the displacement of the printing table. Second, previous studies showed that partially melted metallic powder grains or pores formed by the collapse during the sintering process contribute to an irregular surface morphology,[26] although the present 3D disk samples did not show this pattern.

The Ti3DP surface topography led to a rough surface (7.76 ± 0.89 μm), which was approximately 40 times higher than the machined samples (0.197 ± 0.06 μm); nevertheless, the printed surface was less hydrophilic. This is expected because commonly higher wettability is anticipated on less rough surfaces.[30] Regarding surface roughness, establishing a topography with nanostructures and microgrooves seems to be a promising choice for the design of the implant neck or transmucosal component.[31] Thus, smoother surfaces (Ra < 0.2 μm) tend to have reduced connective tissue adhesion, while favoring epithelial cell adhesion.[3,32] Typically, 3D-printing techniques employing selective laser sintering produce devices with rough surfaces. According to the reports by Guo *et al.*,[21] the 3D-printed titanium samples exhibited higher roughness than the machined samples (Ra of 6.57 vs 0.01 μm), but with similar wettability (contact angle of 63.79° vs 79.76°, respectively), resulting in a more favorable surface for cellular adhesion and proliferation due to roughness.

Titanium substrates with microgrooves and controlled roughness have been shown to induce changes in fibroblast gene expression, impacting their morphology, cellular adhesion, and various biological activities such as cell signaling, transcription, translation, and extracellular matrix production.[33] However, there is still no

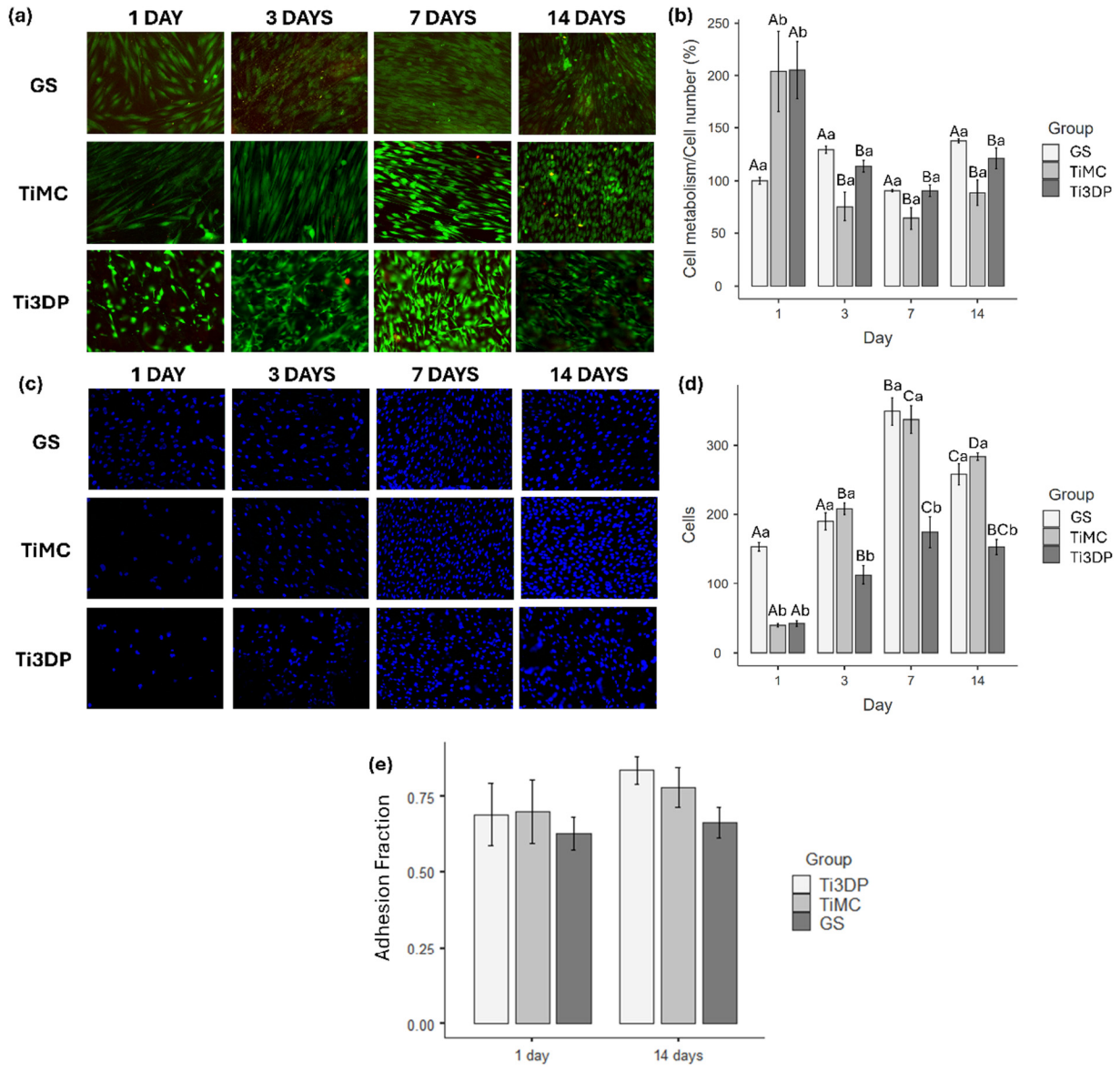

FIG. 5. (a) Representative images of the Live/Dead assay (20× magnification). Live cells = green; dead cells = red; (b) Bar graph representing the cell metabolism per cell. The data were normalized based on the result of day 1 in the GS group, considered as 100%. Capital letters allow for comparisons among the time points for each experimental group. Lowercase letters allow for comparisons between experimental groups within each time point. Different letters indicate statistically significant differences (two-way ANOVA post-hoc Tukey's test; $p < 0.05$; $n = 6$); (c) Representative images of cell density on the surface of glass coverslips (GS), machined titanium disks (TiMC), and 3D-printed titanium disks (3DP). Blue = nucleus (DAPI). Magnification of 20×; (d) bar graph representing the mean number of cells. Capital letters allow for comparisons among the time points for each experimental group. Lowercase letters allow for comparisons between the experimental groups within each time point. Different letters indicate statistically significant differences (two-way ANOVA post-hoc Tukey's test; $p < 0.05$; $n = 6$). (e) Bar graph representing the adhesion fraction. No difference was found between the groups or evaluation period (two-way ANOVA post-hoc Tukey's test; $p > 0.05$; $n = 6$).

consensus in the literature regarding the effectiveness of the superficial treatment of transmucosal components to enhance fibroblast adhesion and proliferation. Therefore, we seeded Ti3DP and TiMC samples with HGFs to evaluate cell dynamics and collagen expression. Cells seeded onto GS were used as controls, as previously proposed in the literature, since the glass surface allows cell adhesion with flat 2D cytoskeleton architecture.[34,35] According to the results of the current study, the cells were able to attach and remain viable in the Ti3DP group throughout all analysis periods of the Live/Dead assay, such as also observed for the TiMC and GS groups.

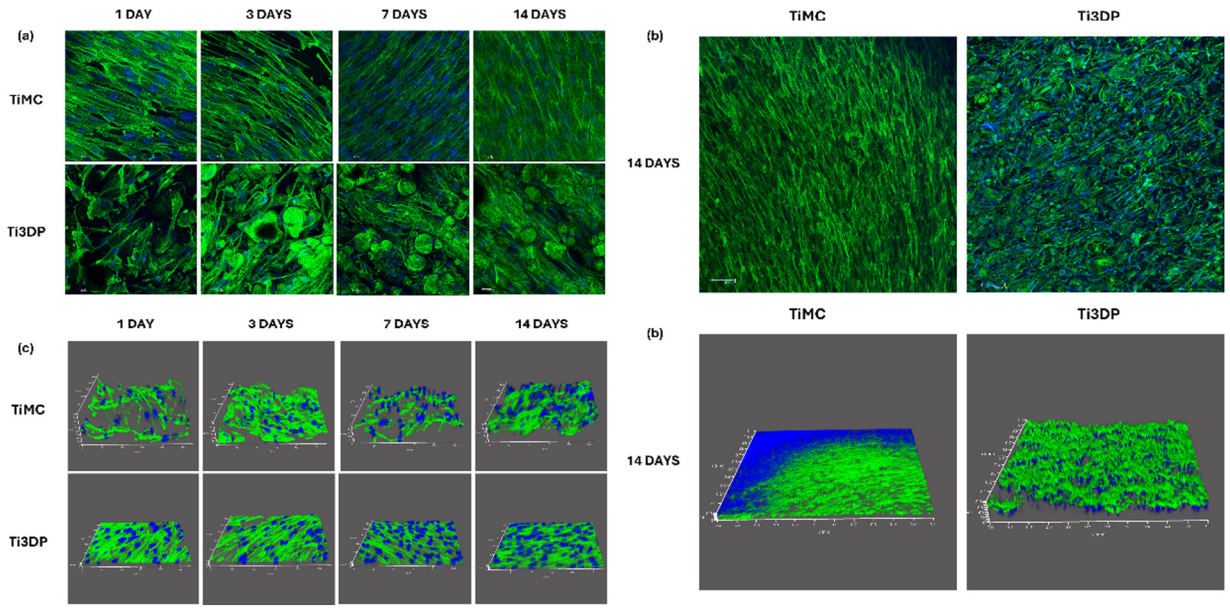

FIG. 6. Adhesion and spreading assay—Immunofluorescence for F-actin. Representative images of the surface of machined titanium disks (TiMC) and 3D-printed disks (3DP). Green = F-actin. Blue = nucleus (DAPI). (a) 40× magnification; (b) 10× magnification; (c) three-dimensional volume rendering, 40× magnification; (d) three-dimensional volume rendering, 40× magnification.

Nevertheless, Hoescht assay denoted that a lower number of cells got attached to TiMC and Ti3DP surfaces in comparison to GS at 1 day. Following 3, 7, and 14 days, the GS and MC groups had similar cell densities, while Ti3DP featured significantly lower cells. As observed in our results, there was an initial increase in cell numbers up to day 7, followed by a reduction at day 14 across all experimental groups, including the GS control. This behavior aligns with the typical dynamics of fibroblast cultures under *in vitro* conditions. During the initial phase, cells proliferate until reaching confluence or near-confluence. After this point, limitations in space and nutrients, along with the accumulation of metabolic by-products in the culture medium, may trigger contact inhibition, reduce proliferation rates, or even lead to a slight decrease in cell number due to cell detachment or apoptosis.[36] Given that this proliferation pattern was consistently observed across all groups, including the GS control, we interpret it as a general biological response to the *in vitro* environment, rather than an effect specifically induced by the material surfaces.

Taking into account the differences among groups on cell number throughout the time points and that these cells were viable, the cell metabolism was normalized by the cell number, and it was noticed that the cells were significantly more metabolic active on titanium substrates (Ti3DP and TiMC) in comparison to GS, possibly reflecting the initial stimulus resulting from titanium contact with the cells. However, in subsequent analysis periods, no

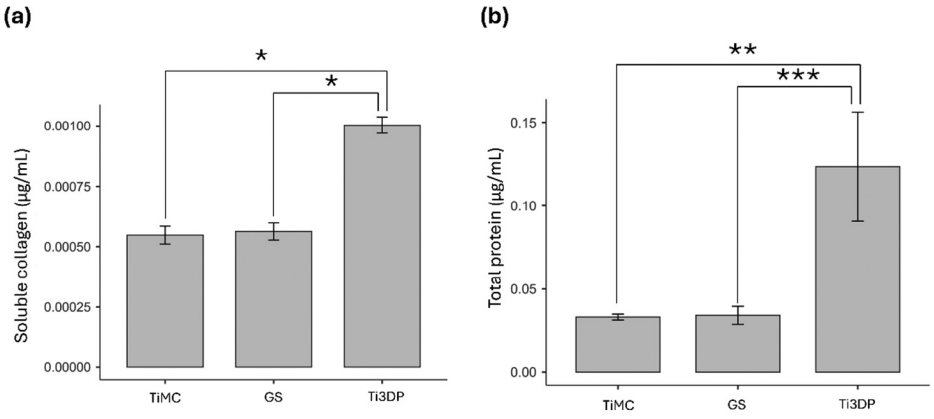

FIG. 7. (a) Bar graph representing soluble collagen present in the cell culture medium. (b) Bar graph representing the total protein concentration (one-way ANOVA post-hoc Tukey's test; *p < 0.01; **p = 0.012; ***p = 0.013; n = 6).

difference in cellular metabolism was observed among groups. In an *in vitro* study, Guo *et al.*[21] concluded that 3D-printed surfaces exhibited a superior proliferation rate (1–7 days) of human gingival fibroblasts compared to those observed on machined surfaces. Scanning electron microscopy images revealed the presence of short filopodia on 3D-printed surfaces after 1 h of incubation, a phenomenon that was not observed in machined samples. Additionally, after 1 day of culture, the cells appeared more spread out and adhered to titanium in the 3D-printed specimens. In turn, Iezzi *et al.*[7] observed that both macro- and microtopography of the 3D-printed implant favored fibroblast adhesion and spreading, compared to the machined implant; however, the difference was not significant, indicating only good biocompatibility. In accordance, Kim *et al.*[22] noted similar values between 3D-printed samples, blasted or not, and machined samples, regarding fibroblast cell adhesion, cell viability, adhesive protein expression (vinculin), and differentiation potential at 14 days.

In the present investigation, clear distinctions in cell morphology and distribution were observed when comparing the groups on F-actin assay. Cells on Ti3DP featured a more 3D morphology while cells on TiMC were flat and with aligned cytoskeleton. Additionally, the adhesion fraction was superior on Ti3DP in comparison to TiMC, besides the fact that no significant difference was observed between these groups. One may suggest that both surfaces are competent in ensuring cellular adhesion even after exposure to mechanical stimuli, with Ti3DP featuring a slightly better behavior. Fibroblasts are anchorage-dependent cells that require adhesion to survive. One of their mechanisms of cellular adhesion occurs through focal adhesion.[36] Focal adhesion is a fundamental process in cell biology, whereby cells connect to the components of the extracellular environment, such as extracellular matrix proteins or proteins adsorbed on solid surfaces.[36] It occurs through specialized structures on the cell membrane called focal points, where cells anchor and maintain intimate contact with the substrate. Thus, cellular adhesion can be influenced by a variety of surface parameters, including characteristics such as hydrophilicity, surface charge, roughness, and surface free energy.[25–27]

Similarly, Yamada *et al.*[37] noted significant differences when assessing cell morphology on smooth titanium surfaces and nanotopographical surfaces. On nanostructured surfaces, the cells exhibited relatively small shapes, accompanied by the development of focal adhesions and well-defined cytoskeletal networks, ensuring good substrate adhesion. Conversely, on smooth surfaces, fibroblasts assumed an elongated fuse-shaped form and established stable adhesions to the substrate. In the present study, a similar distinction in cellular morphology was observed between Ti3DP and TiMC. Like the GS group, cells in the TiMC group displayed a relatively regular fusiform shape, proliferating in a uniform layer. In contrast, cells in the Ti3DP group exhibited spatial distribution at multiple levels and a polymorphic shape, forming a well-defined cytoskeletal network with the presence of multiple lamellipodia and filopodia. Filopodia, composed of parallel actin fibers, serve as sensors to explore the environment, while lamellipodia, composed of branched actin fibers, can withstand traction forces and induce unidirectional cellular displacement by pulling the cell body in the direction of the lamellipodia.[37] This difference suggests that fibroblasts in the Ti3DP group were more mobile than those in the TiMC and GS groups.

The peri-implant connective tissue comprises cells, predominantly fibroblasts, and an extracellular matrix. Fibroblasts produce the primary fibrous proteins constituting the extracellular matrix, such as collagen, elastin, fibronectin, and laminin.[38] Collagen represents a major component of the connective tissue, constituting up to 30% of the total protein mass of the extracellular matrix.[38] Moreover, it plays a crucial role in providing tensile strength, regulating cell adhesion, supporting chemotaxis and cell migration, and directing tissue development.[39] For this reason, this study conducted an analysis of collagen production to investigate the ability of gingival cells to secrete and synthesize a functional extracellular matrix.[14] Thus, the volume of collagen produced by fibroblasts is a significant parameter to consider when contemplating peri-implant sealing. In this regard, the Ti3DP group exhibited clear superiority over the other surfaces. These results are in agreement with Iezzi *et al.*,[7] who concluded that 3D-printed implants showed a significant increase in gene expression such as COL1 and FN1 after 10 days of culture, accompanied by a slightly higher collagen production.

Surface modifications can enhance the gene expression level of the primary components of the connective tissue, such as collagen fibers (types I and III) and elastic fibers (elastin and fibrillin).[37] While some evidence supports higher collagen production on rougher surfaces,[37] other studies do not find this correlation.[38,40] However, as emphasized by de Souza *et al.*,[40] it is crucial to note that the differences in cell type, cell cycle phase, and chemical composition and topography of the material surface can influence the results. Therefore, these variables may yield varying results among studies and should be carefully considered when interpreting the published findings.

Finally, it is worth noting that this study has limitations that should be addressed in future experiments. One of them is the lack of a group with 3D-printed samples without any type of additional postprinting surface modification. Thus, it was not possible to isolate the effect generated solely by the printing process, but rather the synergistic action of the entire chain of surface conditioning processes to which the samples were subjected. Additionally, it was not feasible to develop different printing patterns other than those established by the manufacturer due to limitations in accessing a metal sintering 3D-printer. Different variations in the printing steps and printing angle could have significant impacts over cell metabolism.

Another important aspect is that the present work focused on the initial biological response under *in vitro* conditions. Therefore, factors such as corrosion behavior and possible ion release from the metallic substrates were not evaluated. Although the substrates used are compliant with the medical-grade standards and no cytotoxic effects were observed, future investigations, including ion release assessments, may further clarify the role of chemical factors in modulating cell behavior. Additionally, it is also important to note that focal adhesion was not directly assessed in this study. However, cell adhesion was indirectly evaluated by quantifying cellular activity before and after exposure to a mechanical agitation stimulus. This approach allowed us to infer the strength of cell attachment to the different surfaces. While the molecular characterization of focal adhesion contacts, such as vinculin staining, could offer more detailed insights, it was not included in the original experimental design and thus represents a relevant direction for future studies.

V. CONCLUSION

In alignment with prior research,[10,20–22,24,26,41] it becomes evident that the 3D-printing process stands as a promising avenue to produce transmucosal components. This method exhibits favorable outcomes such as acceptable cellular viability and adhesion, alongside an augmentation in collagen and total protein deposition. These results suggest that the 3D-printed surface has the potential to establish a more intimate and stable interface with the supracrestal connective tissue, which, in turn, could benefit the stability of peri-implant tissues. Thus, it could be possible to conceive a transmucosal component with an apical portion featuring the characteristic rough surface of 3D-printing manufacturing, keeping intimate contact with the connective tissue, while the portion in contact with the epithelial tissue could be polished to facilitate epithelial contact and reduce plaque accumulation. However, further investigations using more complex models, like 3D cell culture and animal models, are necessary to delve into a better understanding of parameters like cellular metabolism and microbiological considerations.

ACKNOWLEDGMENTS

This work was supported by the Coordenação de Aperfeiçoamento de Pessoal de Nível Superior—Brasil (CAPES, Finance Code 001) and M3 Health Indústria e Comércio de Produtos Médicos, Odontológicos e Correlatos S.A. (Plenum Bioengenharia, Jundiaí, SP, Brazil). We thank Dr. Márcia Sirlene Zardin Graeff for the technical support provided in acquiring the images using confocal microscopy and Dr. Livia Pilatti and Dr. Sybele Saska for the support regarding samples manufacturing and processing.

AUTHOR DECLARATIONS

Conflict of Interest

The authors have no conflicts to disclose.

Ethics Approval

Ethics approval has been obtained by Ethics Committee on Human Subjects of Bauru School of Dentistry CAAE protocol #53489421.9.0000.5417. The participants gave informed consent before participating in the study.

Author Contributions

Vitor de Todedo Stuani: Conceptualization (equal); Data curation (equal); Formal analysis (equal); Funding acquisition (equal); Investigation (equal); Methodology (equal); Writing – original draft (equal). **Isabela Sanches Pompeo da Silva:** Investigation (equal); Methodology (equal); Writing – review & editing (equal). **Gustavo Gonçalves do Prado Manfredi:** Investigation (equal); Writing – review & editing (equal). **Fernanda Balestrero Cassiano:** Investigation (equal); Writing – review & editing (equal). **Larissa Alamo:** Data curation (equal); Methodology (equal). **Ligia Espoliar Corrêa:** Data curation (equal); Formal analysis (equal); Methodology (equal); Writing – review & editing (equal). **Jamil Awad Shibli:** Conceptualization (equal); Formal analysis (equal); Resources (equal); Writing – original draft (equal). **Carlos Alberto de Souza Costa:** Conceptualization (equal); Formal analysis (equal); Validation (equal); Writing – review & editing (equal). **Diana Gabriela Soares:** Conceptualization (equal); Data curation (equal); Funding acquisition (equal); Methodology (equal); Supervision (equal); Validation (equal); Writing – review & editing (equal).

DATA AVAILABILITY

The data that support the findings of the study are available from the corresponding author upon reasonable request.

REFERENCES

[1]D. Buser, L. Sennerby, and H. De Bruyn, Periodontol. 2000 **73**, 7 (2017).
[2]R. Beckwith and H. Devlin, Int. J. Oral Maxillofac Implants **39**, 206 (2024).
[3]H. W. Jin, S. Noumbissi, and T. G. Wiedemann, J. Funct. Biomater. **15**, 91 (2024).
[4]M. F. Kunrath, C. Garaicoa-Pazmino, P. M. Giraldo-Osorno, A. Haj Mustafa, C. Dahlin, L. Larsson, and F. Asa'ad, J. Periodontal Res. **59**, 1095 (2024).
[5]H. W. Meng, E. Y. Chien, and H. H. Chien, Biomarker Res. **4**, 24 (2016).
[6]T. Linkevicius and J. Vaitelis, Clin. Oral Implants Res. **26**, 139 (2015).
[7]M. D. M. Ferrà-Cañellas, M. A. Llopis-Grimalt, M. Monjo, and J. M. Ramis, Int. J. Mol. Sci. **19**, 2881 (2018).
[8]F. Al Rezk, G. Trimpou, H. C. Lauer, P. Weigl, and N. Krockow, Gen. Dent. **66**, 18 (2018), https://www.agd.org/docs/default-source/self-instruction-(gendent)/genden-jf-18-al-rezk-si414.pdf.
[9]R. Glauser, P. Schüpbach, J. Gottlow, and C. H. Hämmerle, Clin. Implant Dent. Relat. Res. **7**, S44 (2005).
[10]C. Mangano, A. Piattelli, A. Scarano, M. Raspanti, J. A. Shibli, F. G. Mangano, and G. Iezzi, Int. J. Periodontics Restor. Dent. **34**, e9 (2014).
[11]M. N. Abdallah, Z. Badran, O. Ciobanu, N. Hamdan, and F. Tamimi, Adv. Healthc Mater. **6**, 1700549 (2017).
[12]G. Iezzi, B. Zavan, M. Petrini, L. Ferroni, T. V. Pierfelice, U. D'Amora, Alfredo Ronca, Emira D'Amico, and Carlo Mangano, J. Dent. **140**, 104778 (2024).
[13]H. J. Lee, J. Lee, J. T. Lee, J. S. Hong, B. S. Lim, H. J. Park, Young-Kwang Kim, and Tae-Il Kim, J. Periodontal Implant Sci. **45**, 120 (2015).
[14]Y. Wang, Y. Zhang, D. Jing, Y. Shuang, and R. J. Miron, Clin. Oral Invest. **20**, 685 (2016).
[15]L. A. Roth, M. F. Bastos, M. A. Melo, V. A. R. Barão, R. C. Costa, G. Giro, J. G. S. Souza, K. Grzech-Leśniak, and J. A. Shibli, Life **12**, 937 (2022).
[16]J. Cao, T. Wang, Y. Pu, Z. Tang, and H. Meng, Arch. Oral Biol. **87**, 204 (2018).
[17]A. A. Çomut, H. P. Weber, S. Shortkroff, F. Z. Cui, and M. Spector, Clin. Oral Implants Res. **12**, 433 (2001).
[18]M. Baus-Dominguez, S. Maza-Solano, C. Vázquez-Pachón, M. Flores-Cerero, D. Torres-Lagares, M. Á. Serrera-Figallo, and L. Macías-García, Polymers **15**, 3321 (2023).
[19]M. Degidi, L. Artese, A. Piattelli, A. Scarano, J. A. Shibli, M. Piccirilli, Vittoria Perrotti, and Giovanna Iezzi, Clin. Oral Invest. **16**, 857 (2012).
[20]S. Barui, A. K. Panda, S. Naskar, R. Kuppuraj, S. Basu, and B. Basu, Biomaterials **213**, 119212 (2019).
[21]Y. Guo, X. Wang, C. Wang, and S. Chen, J. Mater. Sci.: Mater. Med. **33**, 27 (2022).
[22]J. H. Kim *et al.*, Dent. Mater. **36**, 945 (2020).
[23]F. Mangano, F. Luongo, J. A. Shibli, S. Anil, and C. Mangano, Int. J. Dent. **2014**, 252343 (2014).
[24]J. Vaithilingam, E. Prina, R. D. Goodridge, R. J. M. Hague, S. Edmondson, F. A. J. Rose, and Steven D. R. Christie, Mater. Sci. Eng. C **67**, 294 (2016).
[25]R. Żebrowski, M. Walczak, A. Korga, M. Iwan, and M. Szala, J. Healthcare Eng. **2019**, 1.

[26]M. Benedetti, E. Torresani, M. Leoni, V. Fontanari, M. Bandini, C. Pederzolli, and C. Potrich, J. Mech. Behav. Biomed. Mater. **71**, 295 (2017).
[27]J. T. Tuomi, R. V. Björkstrand, M. L. Pernu, M. V. J. Salmi, E. I. Huotilainen, J. E. H. Wolff, Pekka K. Vallittu, and Antti A. Mäkitie, J. Mater. Sci.: Mater. Med. **28**, 53 (2017).
[28]J. A. Shibli, C. Mangano, F. Mangano, O. Brasil, B. Lins, F. Cozzolino, and A. Piattelli, Poseido **1**, 45 (2013), http://www.poseido.info/publication/volume-1-2013/poseido-201313149-56-shibli.pdf.
[29]S. Tunchel, A. Blay, R. Kolerman, E. Mijiritsky, and J. A. Shibli, Int. J. Dent. **2016**, 8590971 (2016).
[30]F. P. Nothdurft, D. Fontana, S. Ruppenthal, A. May, C. Aktas, Y. Mehraein, Peter Lipp, and Lars Kaestner, Clin. Implant Dent. Relat. Res. **17**, 1237 (2015).
[31]P. Zhou, F. Mao, F. He, Y. Han, H. Li, J. Chen, and Shicheng Wei, Colloids Surf. B **178**, 515 (2019).
[32]B. G. R. Zigterman, C. Van den Borre, A. Braem, and M. Y. Mommaerts, Biointerphases **14**, 040802 (2019).
[33]M. J. Dalby, M. O. Riehle, S. J. Yarwood, C. D. W. Wilkinson, and A. S. G. Curtis, Exp. Cell Res. **284**, 272 (2003).
[34]L. Alamo, F. B. Cassiano, E. A. F. Bordini, V. T. Stuani, L. E. Pacheco, M. O. Gallinari, C. A. Souza Costa, R. F. L. Mondelli, and D. G. Soares, J. Prosthet. Dent. **132**, 251 (2022).
[35]F. G. Basso, T. N. Pansani, D. G. Soares, L. M. Cardoso, J. Hebling, and C. A. de Souza Costa, Clin. Oral Invest. **22**, 893 (2018).
[36]M. Hamdan, L. Blanco, A. Khraisat, and I. F. Tresguerres, Clin. Implant Dent. Relat. Res. **8**, 32 (2006).
[37]M. Yamada, E. Kato, A. Yamamoto, and K. Sakurai, Biomed. Mater. **11**, 015010 (2016).
[38]L. Ramaglia, G. Di Spigna, G. Capece, C. Sbordone, S. Salzano, and L. Postiglione, Clin. Oral Invest. **19**, 2245 (2015).
[39]T. Rozario and D. W. DeSimone, Dev. Biol. **341**, 126 (2010).
[40]V. Z. de Souza, R. Manfro, J. C. Joly, C. N. Elias, D. C. Peruzzo, M. H. Napimoga, and Elizabeth Ferreira Martinez, Int. J. Implant Dent. **5**, 41 (2019).
[41]A. Bernhardt, J. Schneider, A. Schroeder, K. Papadopoulous, E. Lopez, F. Brückner, and Ute Botzenhart, Mater. Sci. Eng. C **119**, 111631 (2021).